Fluid Dynamics Associated with Body Impact

B. W. Skews[1][†] and B. Ndebele[2]

[1.] *Flow Research Unit, School of Mechanical, Industrial and Aeronautical Engineering, University of the Witwatersrand, Johannesburg, South Africa*
[2.] *CSIR, Department of Mining, Manufacturing, Defense, and Security. Meiring road, Brummeria, Pretoria, South Africa*

† *Corresponding Author Email*: *beric.skews@wits.ac.za*

ABSTRACT

Experiments and numerical simulations were conducted in order to examine the flow field surrounding a flat-faced body impacting on a flat surface. In the experiments impact velocities ranged up to nearly 5 m/s. Visualisation was with a standard z-format schlieren system using a high-speed camera. The associated flow field exhibited ejected gas jets, shed vortices and weak compression waves in the external flow, as well as in the gap depending on pressure differences between the gap and the external field. A computational fluid dynamic simulation (CFD) was undertaken, enabling detailed evaluation of: the flow in the gap, the flow of the emerging jet near the impacting surface, and the development of the wave system and flow on the upper and lower surfaces of the impactor during its descent. It was found that very high pressures are generated in the gap between the impactor and impacting surface and that the jet emerging from the periphery of the impactor can reach supersonic velocities.

Keywords: Compressible flow; Transient jets; Shed vortices.

1. INTRODUCTION

When considering the effects of the impact of a body on another it is usual to consider material properties, the resulting forces that are generated, and body deformation and damage. Treatment of any influence on the surrounding fluid medium are not generally pursued other than in some cases as indicated below. A literature survey on the subject of 'impact' identifies a number of areas where the associated fluid flow is considered. The majority of these cover impact between a body and a liquid. A significant topic is that of a liquid drop impacting on a surface, recently reviewed in Josserand and Thoroddsen (2016). A feature similar to that found in the current study is the lateral formation of a jet. A more general case is that of hull slamming which refers to ship design and the impact of the hull as it enters the water, reviewed in Abrate (2011). These cases all involve complex geometries and, in contrast, Mayer and Krechetnikov (2018) considers the case of a flat plate impacting on a surface, similar to the current study but with the surface being water. This work specifically identifies the jetting that occurs at the periphery and the influence of viscosity and surface tension but unlike the current study the fluid is considered as being incompressible. Marked effects occur when the gap between the bodies is small, of the order of a few millimetres, as occurs in the current work. There is a transient study, with a similar experimental arrangement with surfaces approaching each other Lang *et al.* (2019), for investigating some industrial applications such as squeeze dampers and joint lubrication, examining effects as the gap closes. However, the fluid used is an incompressible liquid and the flow is dominated by viscous effects. An interesting case using a compressible fluid is given by Prausová *et al.* (2019). This is a two-dimensional plane flow between parallel plates with a 2 mm gap height. The results show a typical supersonic under-expanded jet

emerging from the gap, as in the present case, but with the difference being that the flow is steady.

Recent exceptions to the above, which deal with both transient impact and compressible gas flows are the following two studies. A study by Hargather *et al.* (2010) which, by using sensitive optical methods and high-speed imaging, examined the unsteady wave patterns generated dealing with the production of loud sounds and weak shocks. These ranged from clapping of hands to snapping a flexible ruler on a surface. The sudden ejection of air between the surfaces results in sufficient density changes to enable visualisation. Hornung and Cohen (2009), using a theoretical approach, showed that a very strong jet can emerge from between two colliding plates that could drive a strong shock ahead of it. The current experimental work considers the flow developed following the axial impact of flat-faced cylindrical bodies onto a flat surface under different impact velocities. Some of the experimental results have been presented at a conference (Skews and Martinescu (2019)) and are included in this paper, with permission.

As an illustration of the impacting flexible ruler case mentioned in Hargather *et al.* (2010) , this case has been replicated and is shown in Fig.1 in more detail, to show typical features that are encountered. The ruler is held against the surface on the left edge with the right edge lifted and then released. In the first frame there is an indication of an increased density front immediately in front of it. In the next two frames a jet of air is expelled from the sides, denoted as 1, which propagates forwards as the gap decreases. In frame d the front tip of the ruler has nearly reached the surface and two additional features are evident: a transverse wave, marked 2, being driven ahead of the impulsively emerging jet, and a feature at the front tip of the ruler, marked 3, as the air emerges there. In frame e the transverse wave propagates outwards and a strong wave, 4, emerges from the front edge. In frame f a further wave emerges, followed by a number of additional waves shown in the last row.

2. APPARATUS

A sketch of the experimental rig is given in Fig.2. Two aluminium impactors with diameters of 125 mm and 150 mm were used, having flat impact surfaces and 75 mm thickness. The impactors are attached to a spring-loaded shaft. The amount of compression of the spring, and associated distance of the impactor above the impact

surface, was controlled by a release pin passing through a series of holes in the shaft. Extracting the pin resulted in the impactor descending. The impact surface consisted of a 30 x 30 cm, 10 mm thick hard-rubber sheet on top of a wooden surface and a 3 mm thick hardboard sheet. The thickness of the impactor gave a scale to the images. By analysing a number of frames the average height in the images was found to be 158.5 ± 1.5 pixels, thus a scaling factor of 0.47319 mm/pixel. With the frame rate of 75000 fps known the velocity of any feature could thus be determined, as given in Skews and Martinescu (2019).
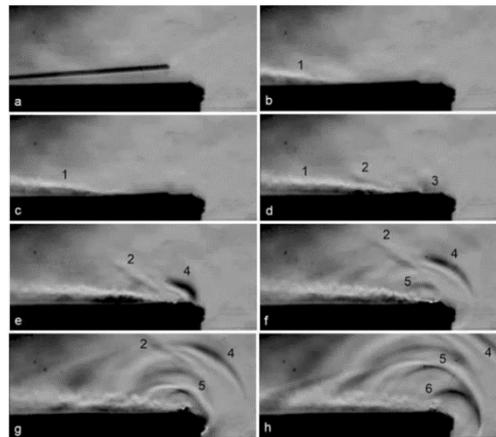
Fig. 1. Flow field resulting from snapping a ruler on a surface.
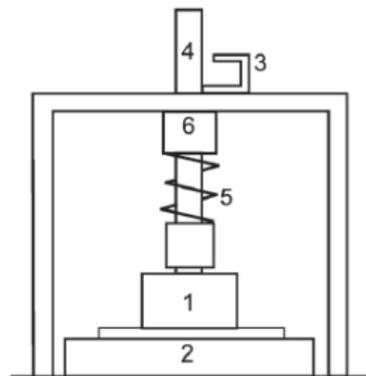
Fig. 2. Rig: 1-impactor, 2-impact surface, 3-release pin, 4-shaft, 5-spring, 6-guide.

3. NUMERICAL MODELING

Computational Fluid Dynamic simulations were run using StarCCM+ 2019.1 Build 14.02.010 (CD–Adapco (2020)) on the Center for High Performance Computing's (CHPC) Lengau cluster. Each node on the cluster is composed of Intel® Xeon® ~CPUs clocked at 2.6 GHz with approximately 100 GB of RAM and 24 cores. Half the geometry is simulated

since the problem is axisymmetric as shown in the following sketches. The overset meshing method was used, as such the domain (Fig.3) is rectangular with a side length of 0.25m wide and 0.40m high and forms the background mesh; similarly the impactor is enclosed in a square boundary (Fig.4) with side length of 0.125mm. Boundary types are shown in Figs.3 and 4. It is important to make sure that the domain boundaries are sufficiently distanced from the impactor in order to prevent spurious wave reflections re-entering the computational domain.
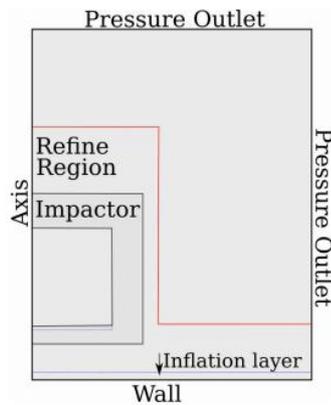
Fig. 3. Impactor in domain.

A quadrilateral dominant mesh was created with express attention given to the floor and impactor bottom (Fig.5). A 0.4mm thick inflation layer composed of 10 layers was created at both the bottom of the impactor and the floor to account for the small gap width that remains at the end of motion.

Implicit unsteady simulations were run, with the impactor falling under the influence of gravity from an initial velocity and height of 50m.s^{-1} and 0.0701m respectively. The fluid around the object was assumed to be an ideal gas, inviscid with ambient pressure and temperature similar to experimental conditions. The CFL (Courant--Friedrichs--Lewy) was set to 100. A time-step was chosen such that the object descended 0.05mm each time. Impactor translation was achieved by assigning a moving reference frame to the impactor-mesh, which frame was moving according to: $u_0 + gt$ where u_0 is the initial velocity, g is gravitational acceleration, and t is cumulative time. When the gap width was 0.4mm, the moving reference speed was set to zero resulting in the impactor stopping. Four stopping criteria were set: an asymptotic stopping criteria, minimum X-momentum and Y-momentum stopping criteria

set at 5×10^{-4} each, and maximum inner iterations set at 100.
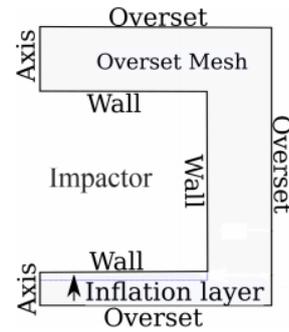
Fig. 4. Impactor.
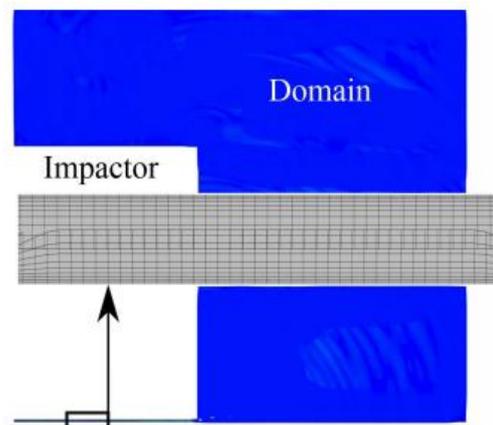
Fig. 5. Gap mesh.

As a measure of mesh independence, the average pressure on the floor was measured at three mesh cell counts (Table 1) after the impactor had fallen 0.035m. Corresponding Grid Convergence Indices (CGI) and discretisation errors were calculated according to Celik *et al*. (2008) and are shown in Table 1. Evidently, the benefits due to further mesh refinement are insignificant as shown by the small relative errors and CGI. As such, the mesh used in Case A, is considered mesh independent.

Table 1 Mesh discretisation error and grid convergence index. Δ represents the average element size, ε the relative error, and *CGI* the grid convergence index

Case	A	B	C
Δ (m)	0.00029	0.00022	0.00017
Cell Count	1147426	1059144	3495209
Pressure	83164.77	83221.77	83222.27
ε	–	0.07%	0.001%
CGI	–	0.1%	0.001%
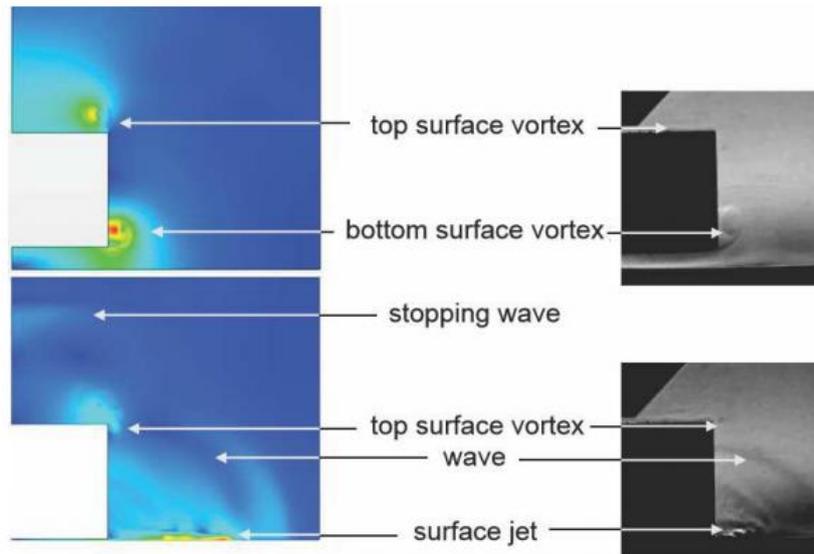
Fig. 6. Overall flow features.

4. OVERALL FEATURES

Figure 6 is a comparison of typical results: simulation on the left (Mach number colouring) and experiment (schlieren imaging) on the right, at the same scale of impactor height.

The top pair are before impact and the lower pair after stoppig. The impact velocity was about 4 m/s for the experiment and about 50 m/s for the simulation; this done in order to show similarity in features. Since in the experiments the bottom face of the compactor and the impacting surface are not perfectly smooth there will always be some gas entrapped between them when the system comes to rest. Also, because of the extremely high pressures developed under the impactor, and depending on its mass, it will decelerate significantly before settling to rest. For this reason a corresponding very small remaining gap is incorporated in the simulations. Correspondingly, the effect of viscous drag is neglected. More importantly, this also accommodates a significant number of computational cells, thereby allowing the flow within the gap to be identified.

As the impactor moves downward, flow passes up the side and separates at the top corner shedding a small toroidal vortex ring. The gas above moves downward together with the top surface, in a wake. At the same time, gas is pushed outward from the bottom surface due to being compressed and flows around the bottom edge with a shear layer and vortex. This remains adjacent to the downward moving impactor surface.

As the impactor comes to rest the top toroidal vortex moves radially outward from the impactor edge and starts moving down towards the impactor side. At the same time the flow following the top surface in the wake also has to suddenly slow down and this results in a compression wave, denoted in Fig.6 as the stopping wave, propagating away from the top surface, bringing the axial flow to rest on the surface.

As the gas between the bottom face of the impactor and the impact surface is squeezed out a strong radial jet is generated, driving a wave outward into the surrounding space. As will be shown later, part of the jet can reach supersonic velocities. This effect was predicted by Hornung and Cohen (2009), who also suggested the possibility of a strong shock wave to be driven ahead of it. Because of the increase in area the current work shows the waves to be weak, and earlier estimates, (Skews and Martinescu 2019), indicate the Mach number averaged over the visible area in the experiment to be as low as Mach 1.04. Further details of the individual features are given below.

5. FLOW FEATURES

5.1 Top and Bottom Surface Vortex Shedding, Before Impact

Details of the evolution of the vortex cross-section on the top surface of the impactor are given in Fig. 7, as obtained from the simulation. Because of the axi-symmetric nature of the flow the schlieren images from the experiment show the toroidal vortex over the whole surface. As the impactor continues

to move downwards the vortex core moves further away from the surface in the developing wake. Once the impactor comes to rest so does the flow adjacent to it, resulting in a wave propagating away bringing the wake flow to rest, denoted as the stopping wave in Fig.6 . The circulation flow around the vortex then moves radially outward over the impactor edge and the core starts moving downward. At the same time the following downward flow towards the surface also starts moving radially outward over the edge with the development of a new shed vortex. The pair of counter rotating vortices then moves away from the side of the impactor.

A toroidal vortex is shed from the bottom surface of the impactor, as shown in Figs.8 and 9. This is influenced by the increasing velocity from the underside as the the gap narrows and fluid is forced out. The exit angle of the shear layer flattens due to increasing exit velocity, and exhibits evidence of developing instabilities. The vortex remains close to the side of the downward moving impactor, and changes shape with the development of instabilities.
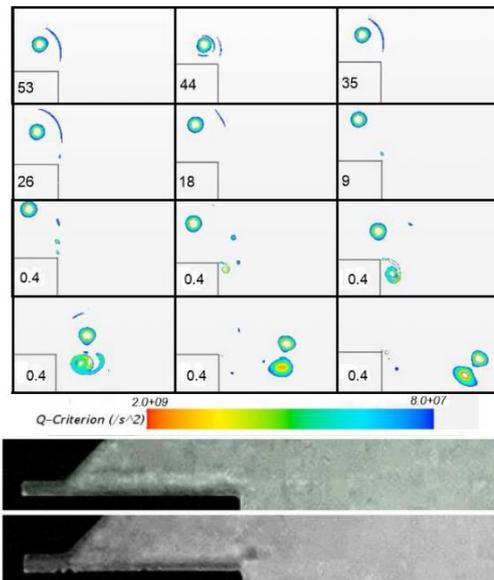
Fig. 7. Vortex development off top surface of impactor.

The variation in flow properties on the two faces of the impactor, before contact with the surface, are given in Fig.10 at different gap widths, corresponding to those in Fig.8. The pressure at the centre of the top face decreases slightly as the gap narrows due to the development of the wake and toroidal vortex. The main influence on the surface pressure

occurs in the vicinity of the vortex. The pressure drops significantly when it is close to the surface and then becomes less marked as it moves away. The pressure on the bottom surface varies as the flow develops, increasing markedly for the much smaller gap width as the gas continues to compress. The Mach number on the top face varies in a corresponding fashion, being lowest immediately under to vortex when it is closer and then increasing significantly in magnitude as it moves away. The Mach number increases steadily as the flow moves out radially, starting at zero on the axis and then for small gaps increasing significantly at the exit.

Numbers refer to gap width in mm, corresponding to time steps of 0.176 ms. Schlieren images from the experiment are before and after impact.
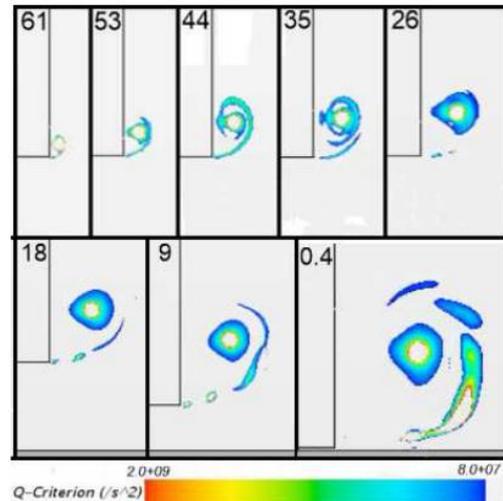
Fig. 8. Vortex development off bottom corner of impactor before impact. Numbers refer to gap width in mm, corresponding to time steps of 0.176 ms. First five images are referenced to bottom of impactor; last three referenced to impact surface.

5.2 External Waves and Surface flow

The initial development of the surface flow from the jet emerging from the gap between the impactor-bottom-surface and the impact surface, is shown in Fig.11. The emerging shear layer shows instabilities with small vortices evident. This breakdown becomes more evident in the second frame with the vortices becoming part of the surface jet. The vortices then become more prominent with increasing density gradient immediately ahead of them. This vortex train is closely associated with the wave system shown below.

A selection of experimental results on wave development are given in Fig.12. The top two rows show the evolution for an impact at 3.6 m/s. There is still a gap between the bottom face of the impactor and the surface. The first image shows the shear layer and indication of the shed vortex as described earlier. In addition, there is the jet of gas on the surface below the shear layer. There is a slight indication of the development of a very weak leading wave, w, which becomes evident in the second frame. This is followed by the emission of a stronger wave, s, passing through the vortex. The waves propagate outwards, becoming weaker as the radius increases. The third row of images show similar effects. The image on the left also indicates small vortices within the main vortex shed from the bottom edge of the impactor.The last row shows the propagation of a strong wave.
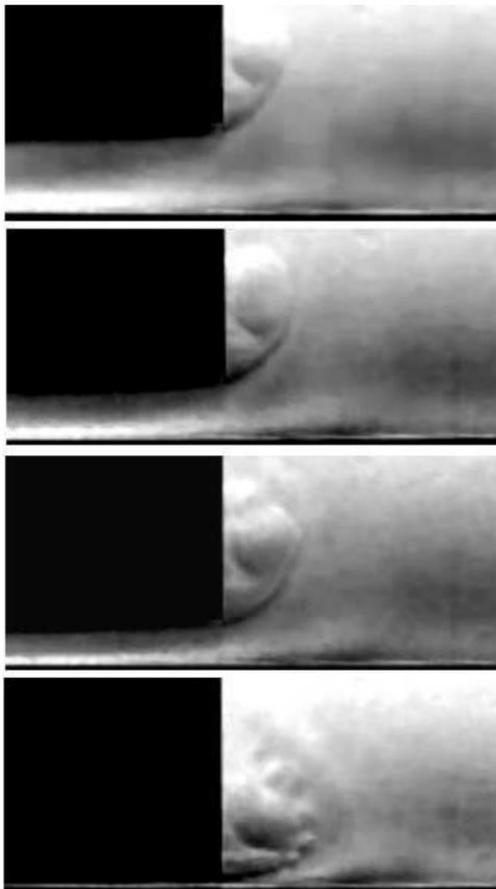
Fig. 9. Schlieren images of bottom edge vortex development. Gap decreasing in 4 mm steps. Impact velocity about 2 m/s.

Further insight is available from the numerical simulation, since details of the surface flow and wave development allows a more detailed study. Impact velocity is much higher than in

the experiments, but as indicated earlier shows the same main features.

Figure 13 shows the early stages of the flow, both under the impactor and along the adjacent surface. The top graph shows conditions when the impactor comes to rest showing the increased pressure in the gap due to the earlier motion. The pressure at the impactor centre reaches a maximum of about 2.4 MPa. The pressure decreases radially due to the outward flow, reaching a pressure of 1.0 MPa at the impactor periphery. This is much higher than the external pressure so the flow expands rapidly to external conditions producing a jet through the gap, as shown in the inset. The small jump in pressure subsequently occurring in the jet is discussed later. The associated Mach number plot shows that the flow is choked at the exit, with the sudden expansion resulting in a supersonic exit flow as suggested in (Hornung and Cohen 2009). This exit flow is very similar to that of an under-expanded jet in steady flow. The associated flood plot of Mach number shows the early development of the feature resulting in the small downstream pressure wave and second Mach number increase, associated with the downstream vortex. The lower pair of graphs in the figure shows conditions 0.02 ms later when the peak in Mach number occurs, increasing to Mach 4.75. The pressure on the axis has dropped to 1.8 MPa because of the exiting flow and fixed gap height, and the exit remains choked. The surrounding exit pressure has also dropped due to the influence of the shed vortex.

Details of the evolution of the surface flow are given in Fig. 14. There is a continual drop in the pressure at the centre of the impactor as flow escapes from the gap. The exit pressure drops correspondingly. However, in Fig. 14c, the external pressure just downstream of the exit is very similar to that at the exit itself, which is still choked. Thereafter the flow changes radically since the gap exit pressure is lower than that in the adjacent external region. This causes the exit to unchoke and a wave to propagate back into the gap; which is treated below. In the second frame there is a strong pressure peak immediately after the exit which may be similar to what happens in a under-expanded nozzle with the development of a downstream shock. All frames, particularly the latter two, show the development of a series of vortices, arising from the initial instability of the shear layer, and which are also identified in the experiment, Fig. 11. They are each followed by an increase in

pressure. The leading one has a spread-out pressure region and corresponds to the very weak leading wave, also identified in experimental images, Fig. 12. The second one, which is the strongest, decreases in strength as it propagates outwards, as is to be expected. It could well be a shock wave corresponding to the experimental result in the bottom row, right hand frames, of Fig. 12. The following pressure peaks correlate with multiple waves noted in the experimentation.
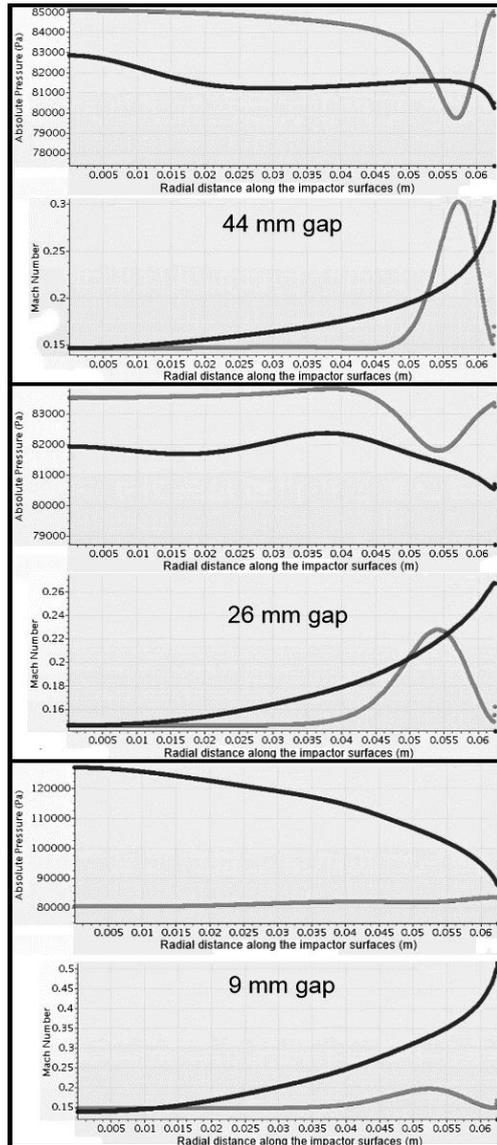
Fig. 10. Pressure and Mach number for the top surface (grey curves) and bottom surface (black curves) before impact. The horizontal sale is from the centre to the impactor edge. 0.36 ms intervals between gap widths.

5.3 Gap Flows

When the pressure to the right of the exit becomes higher than that at the gap exit, a wave propagates back into the gap. This is shown in Figs.15 and 16. This axi-symmetric incident wave implodes towards the centre, followed by increasing pressure as more flow enters through the gap. The initial rise is followed by a compression which causes the wave to steepen as it approaches the centre. The wave is then reflected causing a considerable increase in pressure on the axis. The reflected wave then propagates radially outward, reversing the flow once more. The absolute Mach number plot in Fig.16 gives a clear indication of the positions where the flow reverses, the first frame corresponding to the first frame in Fig.15, and the second frame the corresponding end frame for the reflected wave. The arrows indicate the direction of flow. When the reflected wave reaches the exit it will diffract into the lower pressure surrounding flow. This will result in a further reflected wave back into the gap. It is also likely that there are transverse waves in the gap between the bottom face of the impactor and the underlying surface, which would give rise to the small variations in the recorded pressure.

Fig. 11. Flow emerging from the gap.

6. CONCLUSION

Multiple flow features result when a flat-surfaced impactor moves towards a flat surface. The gas ahead of it is compressed, and vortices develop around the top and bottom surfaces, accompanied by a wake. At small gap distances between the impactor and the surface, radial jets are emitted from the periphery, which can become supersonic. A series of waves

propagate into the external flow caused by the jets on the surface and which are associated with a number of vortices, resulting from instabilities in the shed vortices at the periphery. There are significant changes in the flow within the gap , originally causing the flow to be choked at the exit but which changes as the external pressure drops below that at the exit, resulting in inflow back into the gap.

speed supersonic jets can propagate outward for some considerable distance. These all influence the environment around the impact point with potential hazardous results.
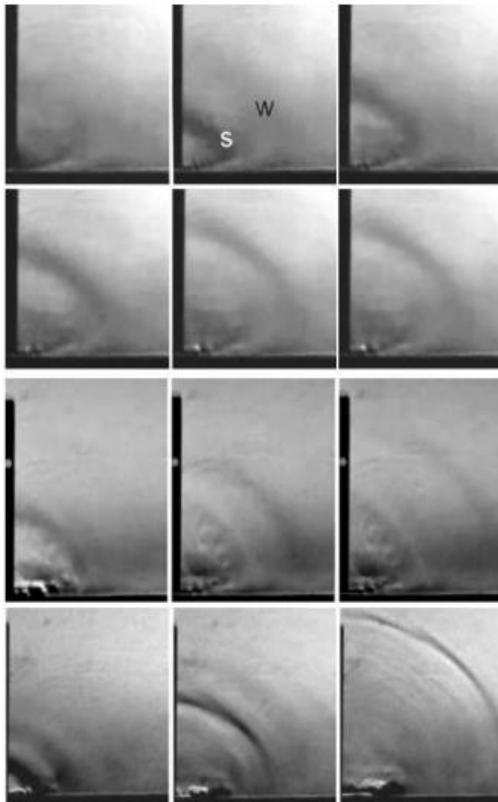
Fig. 12. Schlieren images. Top two rows: 150 mm diameter impactor at 3.6 m/s impact, 0.04 ms intervals. Third row: 150 mm diameter impactor at 2 m/s impact, 0.04 ms intervals; Last row: 125 mm diameter impactor at 3 m/s impact, 0.2 ms intervals.
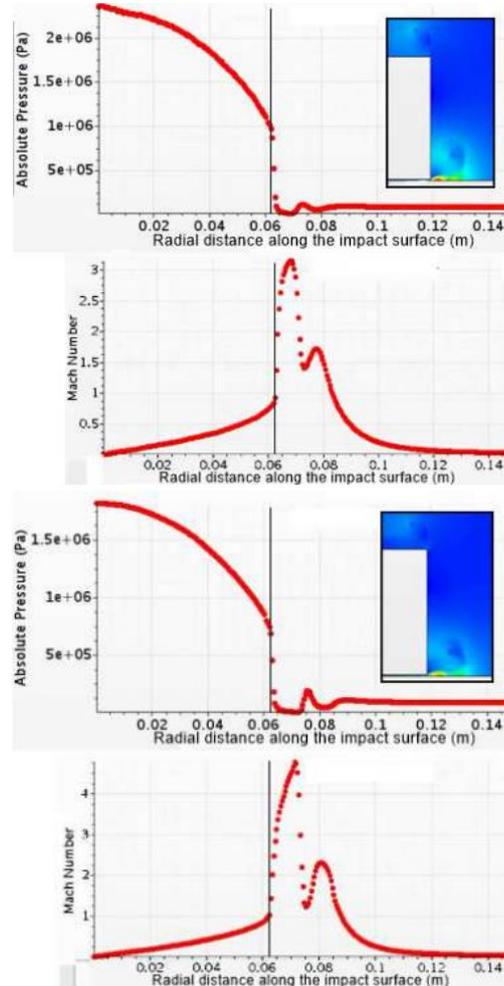
Fig. 13. Flow variation associated with maximum pressure condition (top pair) and highest Mach number condition (bottom pair). Vertical black line shows position of impactor exit

These findings have implications for situations of body impact, particularly in the areas of crash and accident conditions. Because of the high pressure air cushion developed between the impacting body and the impact surface the loading on the surface would be different from that associated with the momentum of the body alone, also taking into account the resulting deceleration of the body before physical contact. Thus it is envisaged to extend the work to account for these effects. In addition there are safety issues related to the resulting external flow. High pressure waves propagate outwards, similar to those from an explosion, and high-

ACKNOWLEDGMENTS
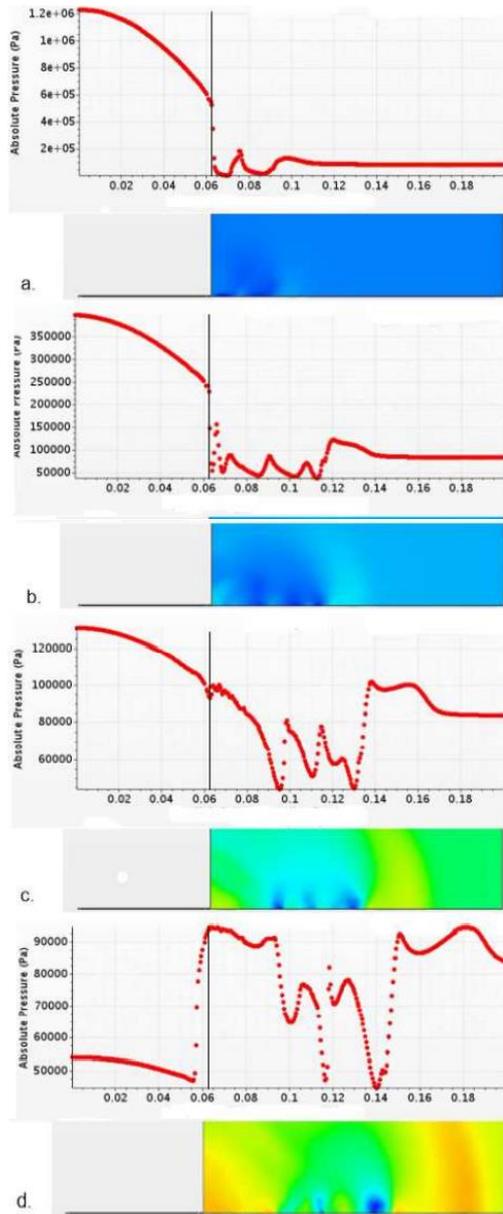
Fig. 14. Evolution of the surface flow. 0.072 ms between images
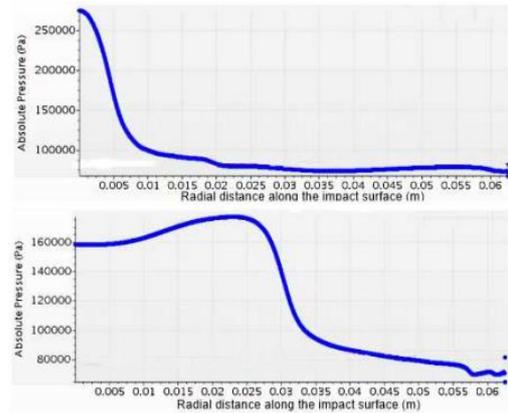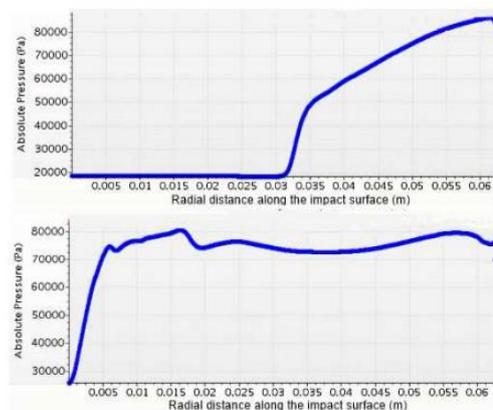
Fig. 15. Pressure variation of the wave in the gap. Top two graphs: entering wave. Bottom two graphs: reflected wave. 0.023 ms between second frame for incident wave and first frame for reflected wave.
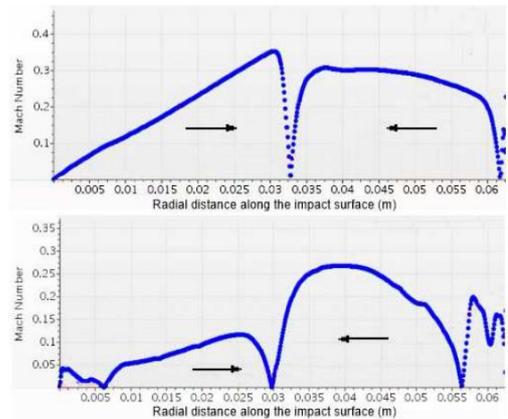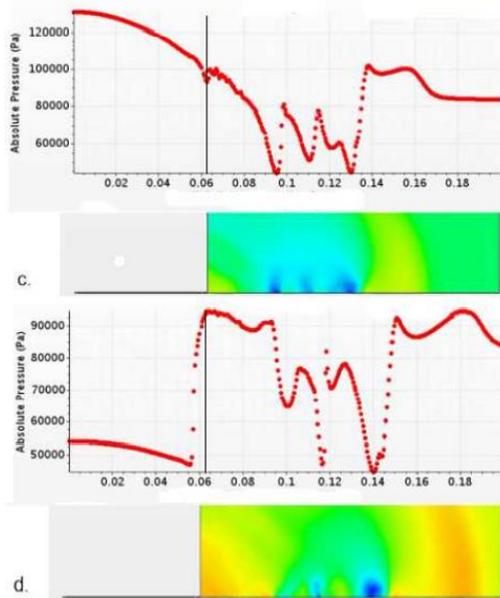
Fig. 16. Absolute Mach number variation in the gap. The figure corresponds to the initial and final frames in Fig.15 corresponding to the incident and reflected waves, with the arrows showing the flow direction.

REFERENCES

Abrate, S. (2011). Hull slamming. *Appl. Mech. Rev. 64(6)*, 060803.

CD–Adapco (2020). *STAR-CCM+ 14.02.010 User Guide*. Melville, NY, USA: CD–Adapco.

Celik, I. B., U. Ghia, P. J. Roache and C. J. Freitas (2008). Procedure for estimation and reporting of uncertainty due to discretization in cfd applications. *ASME Journal of Fluids Engineering 130*(7), 078001.

Hargather, M. J., G. S. Settles and M. J. Madalis (2010). Schlieren imaging of loud sounds and weak shock waves in air near the limit of visibility. *Shock Waves 20*, 9–17.

Hornung, H. G. and D. S. Cohen (2009). On the shock generated by colliding plates in a gas. In I. Krassovkaya (Ed.), *Twenty seventh International Symposium on Shock Waves*, pp. 269. Ioffe Institute.

Josserand, C. and S. T. Thoroddsen (2016). Drop impact on a solid surface. *Annual Review of Fluid Mechanics 48*, 365–391.

Lang, J., R. Nathan and Q. Wu (2019). Experimental study of transient squeezing film flow. *Journal of Fluids Engineering 141*(8), 081110.

Mayer, H. C. and R. Krechetnikov (2018). Flat plate impact on water. *Journal of Fluid Mechanics 850*, 1066–1116.

Prausová, H., O. Bublik, J. Vimmr and J. Hála (2019). Clearance gap flow: simulations by discontinuous galerkin method and experiments. In *EPJ Web of Conferences*, Volume 92, pp. 02073.

Skews, B. and A. Martinescu (2019). Shock waves resulting from body impact. In B. C. Khoo (Ed.), *Thirty second International Symposium on Shock Waves*, pp. 1523–1532. National University of Singapore.